Numerical Evaluation of Fatigue Strength on Mechanical Notched Components under Multiaxial Loadings

Simone Capetta, Roberto Tovo, David Taylor, Paolo Livieri

PII: S0142-1123(10)00243-4
DOI: 10.1016/j.ijfatigue.2010.10.008
Reference: JIJF 2544

To appear in: *International Journal of Fatigue*

Received Date: 15 March 2010
Revised Date: 18 October 2010
Accepted Date: 19 October 2010

Please cite this article as: Capetta, S., Tovo, R., Taylor, D., Livieri, P., Numerical Evaluation of Fatigue Strength on Mechanical Notched Components under Multiaxial Loadings, *International Journal of Fatigue* (2010), doi: 10.1016/j.ijfatigue.2010.10.008

Numerical Evaluation of Fatigue Strength on Mechanical Notched Components under Multiaxial Loadings

Simone Capetta[a], Roberto Tovo[a], David Taylor[b], Paolo Livieri[a]

[a]Department of Engineering, University of Ferrara, Saragat 1, 44100 Ferrara, Italy

[b]Department of Mechanical and Manufacturing Engineering, Trinity College, Dublin 2, Ireland

Corresponding author simone.capetta@unife.it

Abstract

This paper deals with the fatigue behaviour of complex, three-dimensional, stress concentrations under multiaxial loadings. Starting from the stress field obtained by means of a linear elastic analysis and taking advantage of the so-called implicit gradient approach, a safety factor is calculated for high-cycle fatigue. In this first attempt, attention has been focused on the stress-invariant based approaches in the high-cycle fatigue regime. The multiaxial damage evaluation is obtained by analysing the full loading path of the Crossland 5-dimensional invariant deviatoric stress in Euclidean space by means of the variance reference frame. Explicit analytical solutions of the proposed criterion are given in the case of biaxial sinusoidal loads.

The method was validated by comparison with experimental data involving multiaxial in-phase and out-of-phase loading of specimens which contained three-dimensional stress concentrations. These types of stress concentrations are known to present problems for other predictive methods.

Keywords: Implicit gradient, Fatigue, Stress gradient, Multiaxiality.

1. Introduction

Reliability design of real components with three-dimensional (3D) stress concentrations under fatigue loads is a subject of great practical interest to industrial engineers.

3D solid modelling tools are largely used by design engineers for virtual prototyping of new products or structures. In order to reduce computational time, the designer should explore the strategies of modern commercial integrated systems between modelling and FE analysis.

In this context, the structural problems are often complicated due to a multiaxial stress state or to the presence of sharp notches that have a local singular stress field. In order to avoid complicated

calculations, several methods to estimate the fatigue life of notched components under the hypothesis of uniaxial fatigue loading have been proposed over the last few decades. For instance, see Peterson's point method [1] or Neuber's average stress method [2], recently re-considered by Taylor as two important critical distance approaches [3]. Furthermore, we can cite Sheppard's average stress method [4], Lukas and Klesnil's approach based on fracture mechanics [5], the strain-life method [6] and other more recent contributions. Unfortunately, for real structures subjected to complex multiaxial loading conditions, these methods cannot easily be applied directly to each point and the designer must address the procedures in some points where the local stress state appears critical.

Recently, Tovo and Livieri have proposed a new "non-local" design procedure (derived from the *implicit gradient approach*) initially to predict static failure (see [7]) and subsequently to evaluate the stress gradient effect on the fatigue strength of steel welded joints [8]. These methods are called ''non-local" because the strength at a given ''local" point is related to the stress condition of the surrounding material (''non-local") by averaging the stress field obtained. Starting from a stress field obtained from a linear elastic analysis, this method provides a finite reliable solution of a non-local stress all over the investigated solid, as well as at the apex of sharp notches where the stress field is singular. Therefore, by means of the stress gradient approach it is possible to estimate the fatigue lifetime of components with stress raisers without introducing geometrical modifications and by considering a unique design procedure [9]. Note that, as reported in [10], the critical distance approaches can be obtained from the implicit gradient approach, provided that an appropriate weight function is taken into account.

When the local mode I loading is dominant, for welded structures or notched components such as in references [8] and [4], the maximum principal stress was used in defining the failure criterion. However, when a multiaxial stress is present, in order to increase the fatigue lifetime accuracy, a multiaxial criterion should be introduced [11]. Generally speaking, many multiaxial criteria are present in the literature and the choice of a failure criterion should include one of the most common approaches, which are as folows: critical plane-approaches [12-16], energy based approaches [17-19] or stress invariant approaches [20-22]. In this case, stress-invariant based approaches seem to be the most promising criteria in conjunction with the stress gradient problem. In this respect, Cristofori et al. [11] considered the multiaxial criterion proposed in reference [22], based on the use of the amplitude of the second invariant of the deviator $\sqrt{J_{2,a}}$ and the hydrostatic pressure $_{\mathrm{H}}$. In that case, the range of the Crossland invariant stress is in agreement with the range of the von Mises stress because the in-phase proportional loading is considered.

Previous work identified a class of stress concentrations whose fatigue behaviour proved difficult to analyse [23,24]. These features, which were termed "three dimensional stress

concentrations" are characterised by high stress gradients in two orthogonal directions, creating a maximum stress which occurs at a point, rather than along a line as happens in most conventional notched specimens. It was shown that the use of previously-successful methods such as the critical distance approaches [1-3] resulted in highly conservative predictions for this class of notches.

The aim of work described in this paper was to develop a numerical tool in conjunction with three-dimensional modelling tools to be used by industrial engineers. In order to predict the multiaxial fatigue assessment of mechanical components affected by high stress concentrations and complex loading conditions, the implicit gradient approach and a multiaxial fatigue criterion based on the stress invariant approach were used. In order to test the approach under the most severe conditions we chose to use a specimen design which contained one of the above-mentioned three dimensional stress concentration features.

2. Implicit gradient approach

The early works on non-local theory were proposed in 1960 by Kröner [25] and subsequently by Eringen and Edelen [26]. Basically, the idea of a non-local continuum is to consider the stress to be a function of the mean of the strain from a suitable representative volume of the material centered at that point. According to the non-local theory, Pijaudier-Cabot and Bažant [27] introduced the non-local damage concept in order to model strain-softening materials. In particular it was proposed to adopted as non local one scalar variable, e.g. the damage energy release rate, where the non local scalar $\tilde{\zeta}(\bar{x})$ at the point $\bar{x}=(x_1,x_2,x_3)$ in a body with volume V, can be obtained from the weighted average of local scalar $\zeta(\bar{x})$ through the following expression:

$$\tilde{\zeta}(\bar{x}) = \frac{1}{V_r(\bar{x})}\int_V \alpha(\bar{x},\bar{y})\cdot\zeta(\bar{y})\,d\bar{y} \tag{1}$$

In equation (1) $\alpha(\bar{x},\bar{y})$ indicates a scaling of the weight function that depends on the Euclidean distance $\|\bar{x}-\bar{y}\|$ between point $\bar{x}$ and every point $\bar{y}=(y_1,y_2,y_3)$ of V.

Moreover, the reference volume $V_r(\bar{x})$ can be calculated by means of the condition of normalisation of the weight function on the domain V:

$$V_r(\bar{x}) = \int_V \alpha(\bar{x},\bar{y})\,d\bar{y} \tag{2}$$

$V_r(\bar{x})$ is then the integral of the weight function $\alpha(\bar{x},\bar{y})$ extended to the entire volume of the body, so the factor $1/V_r(\bar{x})$ allows, for homogeneous states of stress, the local equivalent tension and the corresponding non-local stress match.

A variant of non-local integral definitions, defined as "implicit gradient model" was initially proposed by Peerlings et al. [28]. In fact, starting from the definition in terms of the non-local model (1), a gradient expansion of the non local scalar could be developed [29]:

$$\tilde{\zeta}\left(\bar{x}\right) \cong \zeta\left(\bar{x}\right) + c^2 \nabla^2 \tilde{\zeta}\left(\bar{x}\right) \tag{3}$$

where *c* is a characteristic length related to the weight function $\alpha(\bar{x},\bar{y})$ defined on the whole volume V. For engineering applications, *c* is assumed to only be related to relevant material properties [7]. In equation (3) the Laplacian operator is applied to the non-local equivalent stress, so that $\tilde{\zeta}\left(\bar{x}\right)$ can be obtained by solving an implicit type differential equation. Usually in this type of analysis only the Neumann-type boundary condition is taken into consideration, expressing the orthogonality of the gradient of the solution sought by the outgoing normal to the edge of the domain of integration:

$$\nabla\tilde{\zeta} \cdot \bar{n} = 0 \tag{4}$$

where $\bar{n}$ is the normal to the surface of the body of volume V [28,30]. In order to obtain the non-local equivalent stress $\tilde{\zeta}\left(\bar{x}\right)$ on a three-dimensional component we need only the material parameter *c*. In this way we avoid to estimate a finite volume based on the results of stress analysis that necessary depends on loading condition and the geometry [31-34]. So that, the non local scalar $\tilde{\zeta}\left(\bar{x}\right)$ in each point of the volume V can be substituted by solving the differential equation (3) because it is much easier to solve numerically than eq. (1). Moreover, implicit gradient approach can be applied to a three-dimensional mechanical component, where the actual critical point cannot be previously assumed but has to be localized by means of numerical investigation. PDE Modes of COMSOL Multiphysics® has been used to solve eq. (3). Second order tetrahedral elements have been employed to mesh the three-dimensional models, as the Neumann-type boundary condition has been applied to all lateral surfaces of the models.

3. Fatigue strength prediction in multiaxial stress field

In this paper, we consider non-proportional, in-phase and out-of-phase, constant amplitude loading. Since, the fatigue behaviour is related to stress variations, in order to correctly interpret stress fields, it must be considered that under non-proportional loading the principal stress directions are not constant. For this reason, it could be necessary to apply a multiaxial criterion together with the stress gradient approach under mixed-mode loadings, in order to correctly perform the high-cycle fatigue damage evaluation. In the following subsections a theoretical introduction to the models of calculation used for this purpose will be presented.

3.1. Definition of the equivalent amplitude of the deviatoric component

From a theoretical point of view, many multiaxial criteria could be used in the implicit gradient approach, namely critical plane approaches, stress-invariant based approaches and integral approaches. In fact, such criteria make use of scalar quantities that can be introduced as equivalent stress in eq. (3).

In this study, multiaxial fatigue damage calculation is performed by means of a stress-invariant based criterion (*PbP* approach) proposed by Cristofori et al. [22,35]. It makes use of the deviatoric component $\bar{\sigma}_d(t)$ and hydrostatic component $\sigma_H(t)$ to evaluate the damage due to generic fatigue loading. The method frame is fully formalised in [22] and hereafter briefly summarised. In order to introduce stress quantities, let us consider a generic time variable stress tensor at a given point:

$$\bar{\bar{\sigma}}(t)=\begin{bmatrix}\sigma_x(t) & \tau_{xy}(t) & \tau_{xz}(t)\\ \tau_{yx}(t) & \sigma_y(t) & \tau_{yz}(t)\\ \tau_{zx}(t) & \tau_{zy}(t) & \sigma_z(t)\end{bmatrix} \tag{5}$$

The stress tensor $\bar{\bar{\sigma}}(t)$ can be split into its deviatoric and spherical parts in the usual way:

$$\bar{\bar{\sigma}}(t)=\bar{\bar{\sigma}}_d(t)+\sigma_H(t)\cdot\bar{\bar{I}} \tag{6}$$

where $\bar{\bar{I}}$ is the second order unit tensor. The hydrostatic stress $\sigma_H(t)$ is a scalar function and its maximal value $\sigma_{H,max}$ over time *T* can be simply calculated as:

$$\sigma_{H,max} = \max_{T}\left[\sigma_H(t)\right] \tag{7}$$

According to the notation used for the Crossland invariant criterion [21], the deviatoric tensor $\bar{\bar{\sigma}}_d(t)$ can be concisely represented as a 5- element vector defined as follows:

$$\bar{s}(t) = \begin{bmatrix} s_1(t) \\ s_2(t) \\ s_3(t) \\ s_4(t) \\ s_5(t) \end{bmatrix} = \begin{bmatrix} \frac{\sqrt{3}}{6}\left(2\sigma_x(t) - \sigma_y(t) - \sigma_z(t)\right) \\ \frac{1}{2}\left(\sigma_y(t) - \sigma_z(t)\right) \\ \tau_{xy}(t) \\ \tau_{xz}(t) \\ \tau_{yz}(t) \end{bmatrix} \tag{8}$$

As an external load is applied the tip of the vector, $\bar{s}(t)$ describes a curve Γ, the deviatoric stress component loading path, as shown in Fig. 1. There are several ways of defining the range of the deviatoric vector so identified in [36] and [37]. The starting point of the *PbP* approach is the hypothesis that the damage related to a generic loading path Γ can be estimated by considering the single contributions $\Gamma_{p,i}$ calculated by projecting the loading path itself along the axes of a frame of reference chosen as a base of the Euclidean space.

In order to propose a procedure suitable for addressing the above problem, the principal axes of path Γ can be attempted to be used in order to define a unique frame of reference, which is suitable when considering the presence of non-zero out-of-phase angles. For this purpose, to correctly calculate the directions of the above principal axes, path Γ can be treated as a continuum, so that, its centroid can be determined as follows[38]:

$$s_{m,i} = \frac{1}{T}\int_T s_i(t)\,dt \quad i = 1,.....,5 \tag{9}$$

where T is the period. Moreover, using a definition similar to the one adopted to define a continuous moment of inertia, the rectangular moments of inertia of path Γ can be represented with respect to its centroid, by using the following symmetric square matrix of order five:

$$C_{ij} = \frac{1}{T}\int_T \left(s_i(t) - s_{m,i}\right)\cdot\left(s_j(t) - s_{m,j}\right)dt \quad i,j = 1,.....,5 \tag{10}$$

This matrix has five eigenvalues and five orthogonal eigenvectors. The eigenvalues are the principal moments of inertia, whereas the eigenvectors are the principal directions of the tensor path, calculated with respect to the centroid itself. Finally, the loading path Γ can be projected along each frame axis (suffix i) so that, the equivalent deviatoric stress amplitude, $\sigma_{d,a}$, can be calculated, in accordance with the *PbP* approach, as follows:

$$\sigma_{d,a} = \sqrt{\sum_i \left(\sigma_{d,a}\right)_i^2} \tag{11}$$

where $(\sigma_{d,a})_i$ is the amplitude of the projection along i^{th} axis.

3.2. Evaluations of non local stress fields

The above procedure allows the assessment of the equivalent deviatoric stress amplitude to be performed. By means of eq. (3), non local stress quantities, linked to fatigue life, can be defined assuming that $\tilde{\sigma}_{d,a}=\xi$ and assuming that the local scalar field is the equivalent deviatoric stress amplitude resulting from an isotropic linear elastic solution $\sigma_{d,a}=\zeta$. Eqs. (3) and (4) become:

$$\tilde{\sigma}_{d,a} \cong \sigma_{d,a} + c^2 \nabla^2 \tilde{\sigma}_{d,a} \tag{12}$$

$$\nabla\left(\tilde{\sigma}_{d,a}\right) \cdot \bar{n} = 0 \tag{13}$$

As mentioned above, the stress invariant based multiaxial criterion, also uses the hydrostatic component $\sigma_H(t)$ to perform the fatigue life estimation so that, the non local scalar stress field of the hydrostatic component in the whole volume V has to be evaluated; in this case eqs. (3) and (4) give:

$$\tilde{\sigma}_{H,max} \cong \sigma_{H,max} + c^2 \nabla^2 \tilde{\sigma}_{H,max} \tag{14}$$

$$\nabla\left(\tilde{\sigma}_{H,max}\right) \cdot \bar{n} = 0 \tag{15}$$

3.3. Multiaxial high-cycle fatigue criteria

Fatigue limit calculation is performed by a biparametric method, similar to the one proposed by Lazzarin and Susmel [39], formulated in terms of stress tension invariants. According to this

approach, fatigue behaviour is related to the multiaxial stress ratio, ρ_{FL}, between the non local values of the hydrostatic component, $\tilde{\sigma}_{H,max}$ and the deviatoric stress component, $\tilde{\sigma}_{d,a}$ [22,35]:

$$\rho_{FL} = \sqrt{3} \cdot \frac{\tilde{\sigma}_{H,max}}{\tilde{\sigma}_{d,a}} \tag{16}$$

For a given loading condition, the estimated fatigue limit value, $\sigma_{d,A}\big|_{\rho_{FL}}$, can be calculated by assuming a linear variation of $\sigma_{d,A}\big|_{\rho_{FL}}$ in respect of ρ_{FL}. Generally, the uniaxial fatigue limit, $\sigma_{d,A}\big|_{\rho_{FL}=1}$ and the torsional fatigue limit $\sigma_{d,A}\big|_{\rho_{FL}=0}$ are used to calibrate the criterion:

$$\sigma_{d,A}\big|_{\rho_{FL}} = \sigma_{d,A}\big|_{\rho_{FL}=0} + \rho_{FL} \cdot \left(\sigma_{d,A}\big|_{\rho_{FL}=0} - \sigma_{d,A}\big|_{\rho_{FL}=1} \right) \tag{17}$$

Finally, the general form for this criterion can be written by comparing the non local value of the deviatoric stress component and the estimated fatigue limit value:

$$\tilde{\sigma}_{d,a} \le \sigma_{d,A}\big|_{\rho_{FL}} \tag{18}$$

4. General procedure of calculation

To clarify this procedure it is important to highlight the fundamental steps that we need to obtain a multiaxial fatigue damage evaluation by means of the aforementioned non local approach in conjunction with the *PbP* criterion. Basically, seven fundamental steps are required to perform the calculation:

1) Linear elastic stress analysis has to be carried out for any external loading applied.

2) Maximum variance reference frame is calculated for any nodal point.

3) Local values of the equivalent deviatoric stress amplitude, $\sigma_{d,a}$, and hydrostatic component, $\sigma_{H,max}$, are evaluated for any nodal point.

4) Non local values of $\tilde{\sigma}_{d,a}$ and $\tilde{\sigma}_{H,max}$ are calculated by means equations 12, 13, 14 and 15 of the implicit gradient approach.

5) Multiaxial stress ratio, ρ_{FL}, between the non local values of the hydrostatic and deviatoric stress components is evaluated.

6) Fatigue limit value, $\sigma_{d,A}\big|_{\rho_{FL}}$, for a given loading condition is calculated by means of eq. (17).

7) Fatigue strength estimation is finally performed at each nodal point by means of eq. (18).

5. Analytical formulas under two sinusoidal loading components

In order to be able to fully implement the above procedure of calculation efficiently, some fundamental quantities have to be expressed by an explicit analytical relationship for high cycle fatigue estimations. In fact in the references [22,35] general definitions are given and the explicit solution is proposed for plane stress loadings.
The aim of this paper is to propose the analytical formulas that will allow us take into account the full stress tensor in the case of a specimen or component loaded by complex conditions. In particular we consider two synchronous sinusoidal loads at most, including a phase angle between the two components. In the following section, the superscripts "′" and "″" refer, respectively, to the stress quantities related to the first and second external loading applied condition.

5.1 Definition of the stress quantities

Let us consider a generic discretisation of the domain V, where *k* is the index of the node and *n* the total number of nodes. By means of a linear stress analysis, the stress tensor $\overline{\overline{\sigma'}}(t,k)$ and $\overline{\overline{\sigma''}}(t,k)$ can be obtained in the node *k* for both loading conditions. Neglecting the dependence on *k* index, the stress tensors components can be expressed as follows:

$$\sigma'_{ij}(t) = \sigma'_{ij,m} + \sigma'_{ij,a}\sin(\omega t) \quad \text{with} \quad i,j = x,y,z \tag{19}$$

$$\sigma''_{ij}(t) = \sigma''_{ij,m} + \sigma''_{ij,a}\sin(\omega t - \varphi) \quad \text{with} \quad i,j = x,y,z \tag{20}$$

where the subscripts *m* and *a* identify the mean value and the amplitude of the stress component *ij* respectively. Finally, φ is the phase angle between load components.

Using Crossland's notation to represent the deviatoric component, the deviatoric vector $\bar{s}(t)$ can be split into vectors $\bar{s}'(t)$ and $\bar{s}''(t)$, which represent the deviatoric component for the first and second external loading condition respectively:

$$\bar{s}(t) = \bar{s}'(t) + \bar{s}''(t) \tag{21}$$

According to the properties of Euclidean space, the vectors $\bar{s}'(t)$ and $\bar{s}''(t)$ can be expressed by the mean values and the amplitudes so that we obtain the following vectors:

$$\bar{s}'(t) = \bar{s}'_m + \bar{s}'_a \cdot \sin(\omega t) \tag{22}$$

$$\bar{s}''(t) = \bar{s}''_m + \bar{s}''_a \cdot \sin(\omega t - \varphi) \tag{23}$$

$$\bar{s}(t) = \bar{s}'(t) + \bar{s}''(t) = \bar{s}'_m + \bar{s}'_a \cdot \sin(\omega t) + \bar{s}''_m + \bar{s}''_a \cdot \sin(\omega t - \varphi) \tag{24}$$

Finally the vectors $\bar{s}'_m$, $\bar{s}'_a$, $\bar{s}''_m$ and $\bar{s}''_a$, by means of stress components, result as follows:

$$\bar{s}'_m = \left[\frac{2\sigma'_{x,m} - \sigma'_{y,m} - \sigma'_{z,m}}{2\sqrt{3}} \;\middle|\; \frac{\sigma'_{y,m} - \sigma'_{z,m}}{2} \;\middle|\; \tau'_{xy,m} \;\middle|\; \tau'_{xz,m} \;\middle|\; \tau'_{yz,m} \right] \tag{25}$$

$$\bar{s}'_a = \left[\frac{2\sigma'_{x,a} - \sigma'_{y,a} - \sigma'_{z,a}}{2\sqrt{3}} \;\middle|\; \frac{\sigma'_{y,a} - \sigma'_{z,a}}{2} \;\middle|\; \tau'_{xy,a} \;\middle|\; \tau'_{xz,a} \;\middle|\; \tau'_{yz,a} \right] \tag{26}$$

$$\bar{s}''_m = \left[\frac{2\sigma''_{x,m} - \sigma''_{y,m} - \sigma''_{z,m}}{2\sqrt{3}} \;\middle|\; \frac{\sigma''_{y,m} - \sigma''_{z,m}}{2} \;\middle|\; \tau''_{xy,m} \;\middle|\; \tau''_{xz,m} \;\middle|\; \tau''_{yz,m} \right] \tag{27}$$

$$\bar{s}''_a = \left[\frac{2\sigma''_{x,a} - \sigma''_{y,a} - \sigma''_{z,a}}{2\sqrt{3}} \;\middle|\; \frac{\sigma''_{y,a} - \sigma''_{z,a}}{2} \;\middle|\; \tau''_{xy,a} \;\middle|\; \tau''_{xz,a} \;\middle|\; \tau''_{yz,a} \right] \tag{28}$$

5.2 Evaluation of the maximum variance reference frame

As mentioned above, the principal directions of the loading path Γ can be used as a reference frame in the deviatoric space in order to perform the calculation of deviatoric component. It should be noted that, the principal directions of path Γ are also the principal directions of the covariance tensor for the same path, so that, the principal axis of the tensor path are coincident with the

directions of maximum variance. To find the direction of maximum variance, the covariance matrix $\overline{\overline{C}}$ can be diagonalised according to an eigenvalue/eigenvector problem. It is important to highlight that the above procedure has to be applied to each node *k* so that the covariance matrix becomes:

$$\overline{\overline{C}}_k = \begin{bmatrix} C_{11,k} & \cdots & C_{1j,k} \\ \vdots & \ddots & \vdots \\ C_{i1,k} & \cdots & C_{ij,k} \end{bmatrix} \quad \begin{matrix} i, j = 1,...,5 \\ k = 1,...,n \end{matrix} \tag{29}$$

where the terms $C_{ij,k}$ are calculated by eq. (10).

The eigenvalue of $\overline{\overline{C}}_k$, say $\lambda_1 \geq \lambda_2$, represents variance terms and defines a diagonal matrix $\overline{\overline{\lambda}}_k$, while the eigenvectors $\overline{n_i^*}$ are collected as columns of a matrix $\overline{\overline{N}}_k$, and the following relation holds:

$$\overline{\overline{C}}_k = \overline{\overline{N}}_k \cdot \overline{\overline{\lambda}}_k \cdot \overline{\overline{N}}_k^{-1} \tag{30}$$

where the matrices $\overline{\overline{\lambda}}_k$ and $\overline{\overline{N}}_k$ are:

$$\overline{\overline{\lambda}}_k = \begin{bmatrix} \lambda_1 & 0 & \cdots & 0 \\ 0 & \lambda_2 & & \vdots \\ \vdots & & \ddots & 0 \\ 0 & \cdots & 0 & \lambda_5 \end{bmatrix} \tag{31}$$

$$\overline{\overline{N}}_k = \begin{bmatrix} \overline{n_1^*} & \cdots & \overline{n_5^*} \end{bmatrix} \tag{32}$$

In other words, diagonalisation of matrix $\overline{\overline{C}}_k$ allows an orthonormal basis $\{\overline{n_1^*}, \overline{n_2^*}, \overline{n_3^*}, \overline{n_4^*}, \overline{n_5^*}\}_k$ to be defined at each nodal point *k* of the Euclidean space on which the loading path Γ can be projected as shown in Fig. 2.

5.3 Calculation of the equivalent deviatoric stress amplitude

Using equation 24 for the deviatoric vector $\bar{s}(t)$, its projections $\bar{s}(t)_{\overline{n_i^*}}$ on the maximum variance reference frame result simply by the scalar projection of $\bar{s}(t)$ onto the five directions $\overline{n_i^*}$, see Fig. 3:

$$\bar{s}(t)\Big|_{\bar{n}_i^*} = \left(\frac{\left\langle \bar{s}(t), \bar{n}_i^* \right\rangle}{\left\langle \bar{n}_i^*, \bar{n}_i^* \right\rangle} \cdot \bar{n}_i^* \right)_{i=1,\dots,5} \tag{33}$$

Note that the norm of the versor $\bar{n}_i^*$ is equal to one so that the above equation becomes:

$$\bar{s}(t)\Big|_{\bar{n}_i^*} = \left(\left\langle \bar{s}_m', \bar{n}_i^* \right\rangle + \left\langle \bar{s}_a', \bar{n}_i^* \right\rangle \cdot \sin(\omega t) + \left\langle \bar{s}_m'', \bar{n}_i^* \right\rangle + \left\langle \bar{s}_a'', \bar{n}_i^* \right\rangle \cdot \sin(\omega t - \varphi) \right)_{i=1,\dots,5} \tag{34}$$

The resulting equation is a compound function in terms of elementary function $\sin(\omega t)$. It has two stationary points i.e. relatively extreme over the interval one period T, which can be found by setting the first derivate of eq. (34) to zero:

$$\left(\frac{d\left(\bar{s}(t)\Big|_{\bar{n}_i^*} \right)}{dt} = 0 \right)_{i=1,\dots,5} \tag{35}$$

When eq. (35) is solved, we obtain two solutions $\alpha_{\bar{n}_i^*}$, $\beta_{\bar{n}_i^*}$ for each eigenvector $\bar{n}_i^*$:

$$\alpha_{\bar{n}_i^*} = \arctan\left(-\left(\frac{\left\langle \bar{s}_a', \bar{n}_i^* \right\rangle}{\left\langle \bar{s}_a'', \bar{n}_i^* \right\rangle} \cdot \frac{1}{\sin\varphi} + \frac{1}{\tan\varphi} \right) \right)_{i=1,\dots,5} \tag{36}$$

$$\beta_{\bar{n}_i^*} = \left(\alpha_{\bar{n}_i^*} + \pi \right)_{i=1,\dots,5} \tag{37}$$

In case of phase angle φ or scalar product $\left\langle \bar{s}_a'', \bar{n}_i^* \right\rangle$ equal to zero, the solutions of eq. (35) are given by angles $\alpha_{\bar{n}_i^*} = -\pi/2$ and $\beta_{\bar{n}_i^*} = \pi/2$. The two angle solutions make it possible to calculate the amplitude of the projection along i^{th} axis by simple relationship:

$$\left(\bar{s}\Big|_{\bar{n}_i^*} \right)_a = \left[\left\langle \bar{s}_a', \bar{n}_i^* \right\rangle \cdot \sin\left(\alpha_{\bar{n}_i^*} \right) + \left\langle \bar{s}_a'', \bar{n}_i^* \right\rangle \cdot \sin\left(\alpha_{\bar{n}_i^*} - \varphi \right) \right]_{i=1,\dots,5} \tag{38}$$

Finally, the equivalent deviatoric stress amplitude can be calculated by means eq. (11) where the single projections are given by previous equation:

$$\sigma_{d,a} = \sqrt{\sum_{i=1}^{5} \left(\sigma_{d,a}\right)_i^2} = \sqrt{\left(\sum_{i=1}^{5} \left(\bar{s}\big|_{\bar{n}_i^*} \right)_a^2 \right)} \tag{39}$$

5.4 Simplifications and shortcuts

It is interesting to observe here that some simplifications can be done if we consider the variance properties of a sinusoidal signal. In fact, it is easy to notice that the eigenvalues λ_i of the matrix $\bar{\bar{\lambda}}_k$, represent variance terms of the projections $\bar{s}(t)\big|_{\bar{n}_i^*}$:

$$\lambda_i = V\left(\bar{s}(t)\big|_{\bar{n}_i^*}\right) \tag{40}$$

Moreover, in the case of sinusoidal loading, the variance is proportional to the amplitude of the signal so that the amplitude of the projection along i^{th} axis is given by the following identity:

$$\left(\bar{s}\big|_{\bar{n}_i^*}\right)_a = \sqrt{2 \cdot V\left(\bar{s}(t)\big|_{\bar{n}_i^*}\right)} = \sqrt{2 \cdot \lambda_i} \tag{41}$$

This expression gives an interesting shortcut in order to evaluate the equivalent deviatoric stress amplitude; let us substitute the previous result in eq. (39), the amplitude of the deviatoric component is given by the following simple relationship:

$$\sigma_{d,a} = \sqrt{\left(\sum_{i=1}^{5} \left(\bar{s}\big|_{\bar{n}_i^*} \right)_a^2 \right)} = \sqrt{2 \sum_{i=1}^{5} \lambda_i} \tag{42}$$

Finally, let us consider the invariant properties of a tensor, the equivalent deviatoric stress amplitude turns out to be:

$$\sigma_{d,a} = \sqrt{2\mathrm{tr}\left(\bar{\bar{\lambda}}_k\right)} = \sqrt{2\mathrm{tr}\left(\bar{\bar{C}}_k\right)} \tag{43}$$

5.5 Calculation of the multiaxial stress ratio

In order to calculate the multiaxial stress ratio using a computational method, as above, an analytical formulation of the maximum hydrostatic component has to be defined. The hydrostatic component of the stress tensor is given by:

$$\sigma_H(t)=\frac{1}{3}\mathrm{tr}\left(\overline{\overline{\sigma}}(t)\right)=\frac{1}{3}\left[\mathrm{tr}\left(\overline{\overline{\sigma'}}(t)\right)+\mathrm{tr}\left(\overline{\overline{\sigma''}}(t)\right)\right] \tag{44}$$

Using the mean value and the amplitude of the stress components, the stress tensors $\overline{\overline{\sigma'}}(t)$ and $\overline{\overline{\sigma''}}(t)$ can be split into mean and amplitude stress tensors so the trace matrix results in the following expressions:

$$\mathrm{tr}\left(\overline{\overline{\sigma'}}(t)\right)=\mathrm{tr}\left(\overline{\overline{\sigma'_m}}+\overline{\overline{\sigma'_a}}\cdot\sin(\omega t)\right)=\mathrm{tr}\left(\overline{\overline{\sigma'_m}}\right)+\mathrm{tr}\left(\overline{\overline{\sigma'_a}}\right)\cdot\sin(\omega t) \tag{45}$$

$$\mathrm{tr}\left(\overline{\overline{\sigma''}}(t)\right)=\mathrm{tr}\left(\overline{\overline{\sigma''_m}}+\overline{\overline{\sigma''_a}}\cdot\sin(\omega t-\varphi)\right)=\mathrm{tr}\left(\overline{\overline{\sigma''_m}}\right)+\mathrm{tr}\left(\overline{\overline{\sigma''_a}}\right)\cdot\sin(\omega t-\varphi) \tag{46}$$

By simplifying eq. (44) with previous equations the hydrostatic component turns out to be:

$$\sigma_H(t)=\sigma'_{H,m}+\sigma'_{H,a}\cdot\sin(\omega t)+\sigma''_{H,m}+\sigma''_{H,a}\cdot\sin(\omega t-\varphi) \tag{47}$$

where:

$$\sigma'_{H,m}=\frac{1}{3}\left(\sigma'_{x,m}+\sigma'_{y,m}+\sigma'_{z,m}\right) \tag{48}$$

$$\sigma'_{H,a}=\frac{1}{3}\left(\sigma'_{x,a}+\sigma'_{y,a}+\sigma'_{z,a}\right) \tag{49}$$

$$\sigma''_{H,m}=\frac{1}{3}\left(\sigma''_{x,m}+\sigma''_{y,m}+\sigma''_{z,m}\right) \tag{50}$$

$$\sigma''_{H,a}=\frac{1}{3}\left(\sigma''_{x,a}+\sigma''_{y,a}+\sigma''_{z,a}\right) \tag{51}$$

Imposing the first derivate of eq. (47) equal to zero, it is possible to find the two solutions that represent the stationary points for $\sigma_H(t)$ over a period T:

$$\alpha_{\sigma_H} = \arctan\left(-\left(\frac{\sigma'_{H,a}}{\sigma''_{H,a}} \cdot \frac{1}{\sin\varphi} + \frac{1}{\tan\varphi}\right)\right) \tag{52}$$

$$\beta_{\sigma_H} = \alpha_{\sigma_H} + \pi \tag{53}$$

In this paper, we only consider constant amplitude loading with the load ratio equal to -1 so that, the mean values of the stress components are equal to zero i.e. $\sigma'_{H,m} = \sigma''_{H,m} = 0$ and eq. (47) is given by the following relationship:

$$\sigma_H(t) = \sigma'_{H,a} \cdot \sin(\omega t) + \sigma''_{H,a} \cdot \sin(\omega t - \varphi) \tag{54}$$

Finally, the maximum value of hydrostatic component over a period T results in the following explicit formula:

$$\sigma_{H,max} = \left|\sigma'_{H,a} \cdot \sin\left(\alpha_{\sigma_H}\right) + \sigma''_{H,a} \cdot \sin\left(\alpha_{\sigma_H} - \varphi\right)\right| \tag{55}$$

6. Experimental details and results

In order to check the validity of the fatigue assessment procedure proposed previously, 70 tests were carried out by testing cylindrical 3D-notched specimens with a diameter equal to 8 mm and made of commercial cold-rolled low-carbon steel, En3B. This material has an ultimate tensile strength, σ_{UTS}, equal to 676 MPa, a yield stress, σ_Y, equal to 653 MPa and a Young's modulus equal to 208500 MPa [40]. The geometry of the tested fatigue samples is shown in Fig. 4.

The specimens are characterised by severe stress raisers with root radius equal to 0.03mm. Such specimens were tested under pure tension, pure torsion and mixed tension–torsion loading in-phase and 90° out-of-phase, by imposing a uniaxial and torsional load ratio, R, equal to −1. Under biaxial load, two different ratios, δ, between the amplitudes of the tensile, σ_a, and torsional, τ_a, nominal stress referring to the gross section were considered, that is, $\delta = 1$ and $\delta = \sqrt{3}$. All tests were carried out on an Instron® 8874 servo-hydraulic axial-torsional testing system with an axial cell ±10 KN and a torsion cell of ±100 Nm. All tests were performed under load control, with a frequency ranging from 8 and 16 Hz, as a function of load value. During all fatigue tests, the specimen stiffness was monitored and fatigue failure was defined by 10% stiffness drop, which resulted in cracks, emanating from the tip of the notch, having a length of approximately 1 mm. Fatigue data

and Wohler's curves of all series are shown in Fig. 5, where the data are reported in terms of nominal stress referring to the gross section. In agreement with observed fatigue behaviour, the reference high cycle fatigue strength was extrapolated at $N_A=2\cdot10^6$ cycles. A summary of the results obtained from the experimental investigations of all series is given in Table 1, where *k* denotes the inverse slope of the Wöhler curve.

Fig. 6 shows examples of the crack paths generated on the surfaces of the specimens for various loading conditions.

7. Tools of calculation and numerical results

The flow-chart reported in Fig. 7 summarises the procedure explained above and highlights the numerical software tools used. In particular, the Structural Mechanics Models of COMSOL Multiphysics® was used to perform linear elastic stress analysis and Matlab® was used to calculate the projection system frame, equivalent deviatoric stress amplitude, $\sigma_{d,a}$, and hydrostatic component, $\sigma_{H,max}$, for any nodal point with reference at $2\cdot10^6$ cycles. Finally, PDE Modes of COMSOL Multiphysics® were used to solve eq. (12)-(15) and to perform the fatigue strength estimation. Moreover, to shift between working environments , it was necessary to establish a suitable import and extraction routine of the stress nodal quantities. In order to evaluate the characteristic length *c* in Eqs. (12,14), we have imposed in a plate with central crack, that the non local equivalent deviatoric stress $\tilde{\sigma}_{d,a}$ equal to the estimated fatigue limit $\sigma_{d,A}\big|_{\rho_{FL}}$, in terms of deviatoric components, when the stress intensity factor at crack tip equal the threshold value ΔK_{th}.

The error factor is defined as:

$$E(\%)=\frac{\sigma_{A,exp}-\sigma_{A,fem}}{\sigma_{A,fem}}\times100 \tag{56}$$

Hence, an error factor greater than zero indicates a conservative prediction. The results in terms of tensile and torsional nominal stress amplitude referring to the gross section, are summarised in Table 2. The predictions were extremely good, having an error index always less than 4%. To our knowledge, no other method has been shown to be capable of this level of accuracy when analysing these types of specimens in either uniaxial or multiaxial loading.

In addition, the proposed method is able to assess, at each nodal point P, the value of nominal stress amplitude to be applied in order to have point P in $2\cdot10^6$ cycles strength condition.

The nodal point showing the lower value is the critical point and such a value is the estimated strength of the specimen. The plot of this estimation is given in Fig. 8.

The sub-modelling technique was used to allow use of a refined mesh near the singularity points in order to obtain the convergence of the non local stress field.

The locations of the critical point predicted by FEA also agree with the experimentally-observed crack initiation points shown in Fig.6.

8. Conclusions

In this paper the effects of high stress-concentrations, three-dimensional notches and multiaxial loading conditions on the fatigue behaviour were considered. The stress field was calculated under linear elastic behaviour of the material, and by taking advantage of the application of the implicit gradient approach, a multiaxial criterion based on the Crossland deviatoric stress has been proposed.

The major conclusions obtained from this work can be summarised as follows:

-The devised approach is seen to be highly accurate in estimating high-cycle fatigue damage in mechanical components without assuming the position of the critical point *a priori*. The method can consider the presence of both multiaxial loading and non zero out-of-phase angles.

- The implicit gradient method applied in conjunction with Projection by Projection approach (*PbP)* is capable of analysing complex three-dimensional notches with small root radii.

- The fatigue life estimation technique proposed in this paper is suitable for situations of practical interest where a safety index can be directly obtained from a post-processing of linear-elastic FE models.

8. References

[1] Peterson R.E., Notch sensitivity. In: Sines G, Waisman JL, editors. Metal fatigue. New York: McGraw Hill 1959; 293-306.

[2] Neuber H., Theory of notch stresses. Springer-Verlag, Berlin 1958.

[3] Taylor D., Geometrical effects in fatigue: a unifying theoretical model. Int J Fatigue 1999; 21:413-420.

[4] Sheppard S.D., Field effects in fatigue crack initiation: long fatigue strength. Journal of Mechanical Design 1991; 113:188-194.

[5] Lukas P., Klesnil M., Fatigue limit of notched bodies. Materials Science and Engineering 1978; 34:61-69.

[6] Qilafku G, Azari Z, Kadi N, Gjonaj M, Pluvinage G. Application of a new model proposal for fatigue life prediction on notches and keyseats. Int J Fatigue 1999;21:753–60.

[7] Tovo R., Livieri P., Benvenuti E., An implicit gradient type of static failure criterion for mixed-mode loading. Int J Fract 2006; 141(3):497-511.

[8] Tovo R., Livieri P., An implicit gradient application to fatigue of sharp notches and weldments. Engng Fract Mech 2007; 74:515-26.

[9] Tovo R., Livieri P., A numerical approach to fatigue assessment of spot weld joints. Fatigue Fract. Engng Mater. Struct., Published Online: Jun 29 2010 12:45AM; DOI: 10.1111/j.1460-2695.2010.01488.x

[10] Tovo R., Livieri P., An implicit gradient application to fatigue of complex structures. Engineering Fracture Mechanics 2008; 75:1804-1814.

[11] Cristofori A., Livieri P., Tovo R., An implicit gradient application to fatigue of sharp notches and weldments. International Journal of Fatigue 2009; 31:12–19.

[12] Matake T., An explanation on fatigue limit under combined stress. Bull JSME 1977; 20:257-63.

[13] McDiarmid DL., A shear stress based critical-plane criterion of multiaxial fatigue failure for design and life prediction. Fatigue Fract Eng Mater Struct 1994; 1475–84.

[14] Carpinteri A., Spagnoli A., Multiaxial high-cycle fatigue criterion for hard metals. International Journal of Fatigue 2001; 23:135–45.

[15] Liu Y., Mahadevan S., A unified multiaxial fatigue damage model for isotropic and anisotropic materials. Int J Fatigue 2007; 29:347–59.

[16] Lu Z., Xiang Y., Liu Y., Crack growth-based fatigue-life prediction using an equivalent initial flaw model. Part II: Multiaxial loading. International Journal of Fatigue 2010; 32:376–381.

[17] Ellyin F., Golos K., Trans. ASME. J Engng Mater Technol 1988; 110:63.

[18] Garud Y.S., Proc symp on methods for predicting material life in fatigue. ASME, New York 1979, p.247.

[19] Leis B.N. Trans. ASME 1977; 99:524.

[20] Sines G., Behaviour of metals under complex stresses. Metal Fatigue, In: Sines G, Waisman J, editors. New York: McGraw-Hill; 1959. p. 145-69.

[21] Crossland B., Effect of large hydroscopic pressures on the torsional fatigue strength of an alloy steel. In: Proceedings of international conference on fatigue of metals, London, NewYork, 1956; pp. 138-149.

[22] Cristofori A., Susmel L., Tovo R., A stress invariant based criterion to estimate fatigue damage under multiaxial loading. Int J Fatigue 2008; 30:1646-1658.

[23] Bellett D., Taylor D., Marco S., Mazzeo E., Guillois J., Pircher T., The fatigue behaviour of three-dimensional stress concentrations. Int J Fatigue 2005; 27:207-221.

[24] Bellett D., Taylor D., The effect of crack shape on the fatigue limit of three-dimensional stress concentrations. Int.J.Fatigue 2006; 28:114-123.

[25] Kröner E., Elasticity theory with long-range cohesive forces. Int J Solids Struct 1967; 3:731-742.

[26] Eringen CA, Edelen DGB, On nonlocal elasticity. Int J Eng Sci 1972; 10:233-248.

[27] Pijaudier-Cabot G, Bažant ZP, Nonlocal damage theory. J Engng Mech 1987; 10:1512-1533.

[28] Peerlings RHJ, de Borst R., Brekelmans WAM, de Vree JHP, Gradient enhanced damage for quasibrittle material. Int J Number Methods Eng 1996; 39:3391-3403.

[29] Peerlings RHJ, Enhanced damage modelling for fracture and fatigue. Ph.D. Dissertation 1999; T.U. Eindhoven.

[30] De Borst R., Mühlhaus HB., Gradient dependent plasticity: formulation and algorithmic aspect. Int J Number Methods Eng 1992; 35:521-539.

[31] Sonsino C. M., Kaufmann H., Grubišić V., Transferability of Material Data for the Example of a Randomly Loaded Forged Truck Stub Axle. SAE Technical Paper Series , 970708, 1997-02-24.

[32] Morel F., Palin-Luc T., A non-local theory applied to high cycle multiaxial fatigue. Fatigue & Fracture of Engineering Materials & Structures 2002; 25:649-665.

[33] Palin-Luc T., Lasserre S., An energy based criterion for high cycle multiaxial fatigue. European Journal of Mechanics - A/Solids 1998; 17:237-251.

[34] Qylafku G., Azari Z., Kadi N., Gjonaj M., Pluvinage G., Application of a new model proposal for fatigue life prediction on notches and key-seats. International Journal of Fatigue 1999; 21:753-760.

[35] Cristofori A., Tovo R., An invariant-based approach for high-cycle fatigue calculation. Fatigue Fract Engng Mater Struct 2009; 32:310-324.

[36] Lemaitre J, Chaboche JL. Mechanics of Solids Materials. Cambridge University Press, Cambridge, 1990.

[37] Papadopoulos I.V., Critical Plane Approaches in High-Cycle Fatigue: on the Definition of the Amplitude and Mean Value of the Shear Stress Acting on the Critical Plane. Fatigue Fract Engng Mater Struct 1998; 21:269-285.

[38] Bishop J. E., Characterizing the non-proportional and out-of-phase extent of tensor paths. Fatigue Fract Engng Mater Struct 2000; 23:1019-1032.

[39] Susmel L., Lazzarin P., A bi-parametric Wöhler curve for high cycle multiaxial fatigue assessment. Fatigue Fract Engng Mater Struct 2002; 25:63-78.

[40] Susmel L., Taylor D., The modified Wöhler curve method applied along with the theory of critical distances to estimate finite life of notched components subjected to complex multiaxial loading paths. Fatigue Fract Engng Mater Struct 2008; 31:1047-1064.

Table 1. Summary of the experimental fatigue results in terms of tensile and torsional nominal stress amplitude referring to the gross section.

Series	Loading conditions			No. data	Slope k	Experimental results at $2 \cdot 10^6$ cycles	
	$\delta=\sigma_a/\tau_a$	φ	R			$\sigma_{A,50\%}$ [MPa]	$\tau_{A,50\%}$ [MPa]
Uniaxial	∞	0°	-1	15	3.76	75.7	-
Torsional	0	0°	-1	16	6.87	-	66.1
Biaxial in-phase	1	0°	-1	13	4.98	52.7	52.7
Biaxial out-of-phase	1	90°	-1	11	4.61	52.9	52.9
Biaxial in-phase	$\sqrt{3}$	0°	-1	8	5.67	68.7	39.7
Biaxial out-of-phase	$\sqrt{3}$	90°	-1	7	5.36	66.7	38.5

Table 2. Synthesis of the numerical results in terms of tensile and torsional nominal stress amplitude referring to the gross section.

Series	Loading conditions			Experimental results at $2 \cdot 10^6$ cycles		Fatigue strength prediction at $2 \cdot 10^6$ cycles		Error index	Critical point location		
	$\delta=\sigma_a/\tau_a$	φ	R	$\sigma_{A,50\%}$ [MPa]	$\tau_{A,50\%}$ [MPa]	$\sigma_{A,50\%}$ [MPa]	$\tau_{A,50\%}$ [MPa]	E(%)	x [mm]	y [mm]	z [mm]
Uniaxial	∞	0°	-1	75.7	-	77.5	-	-2.3%	0.00	0.00	0.00
Torsional	0	0°	-1	-	66.1	-	67.5	-2.1%	0.84	0.00	0.85
Biaxial in-phase	1	0°	-1	52.7	52.7	50.8	50.8	3.7%	-0.25	0.00	0.25
Biaxial out-of-phase	1	90°	-1	52.9	52.9	54.3	54.3	-2.6%	-0.00	0.02	0.04
Biaxial in-phase	$\sqrt{3}$	0°	-1	68.7	39.7	66.3	38.3	3.6%	-0.03	0.01	0.06
Biaxial out-of-phase	$\sqrt{3}$	90°	-1	66.7	38.5	66.3	38.3	0.6%	-0.00	0.02	0.04

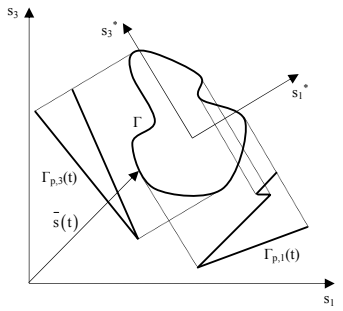

Figure 1. Loading path.

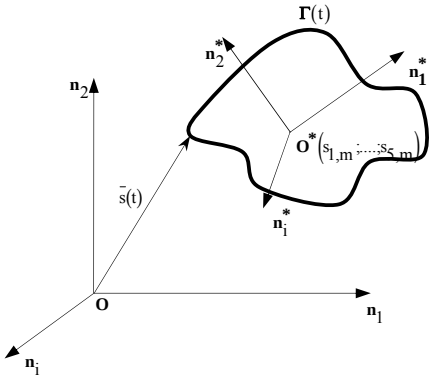

Figure 2. Reference frame.

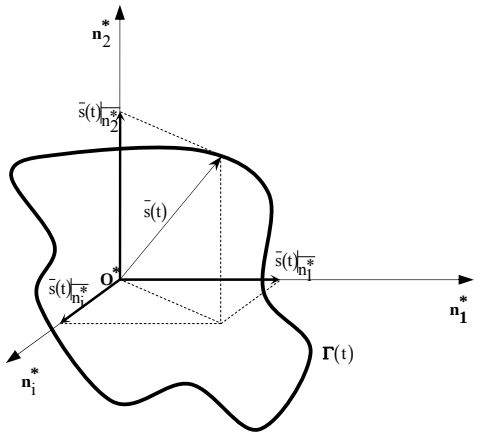

Figure 3. Projected path.

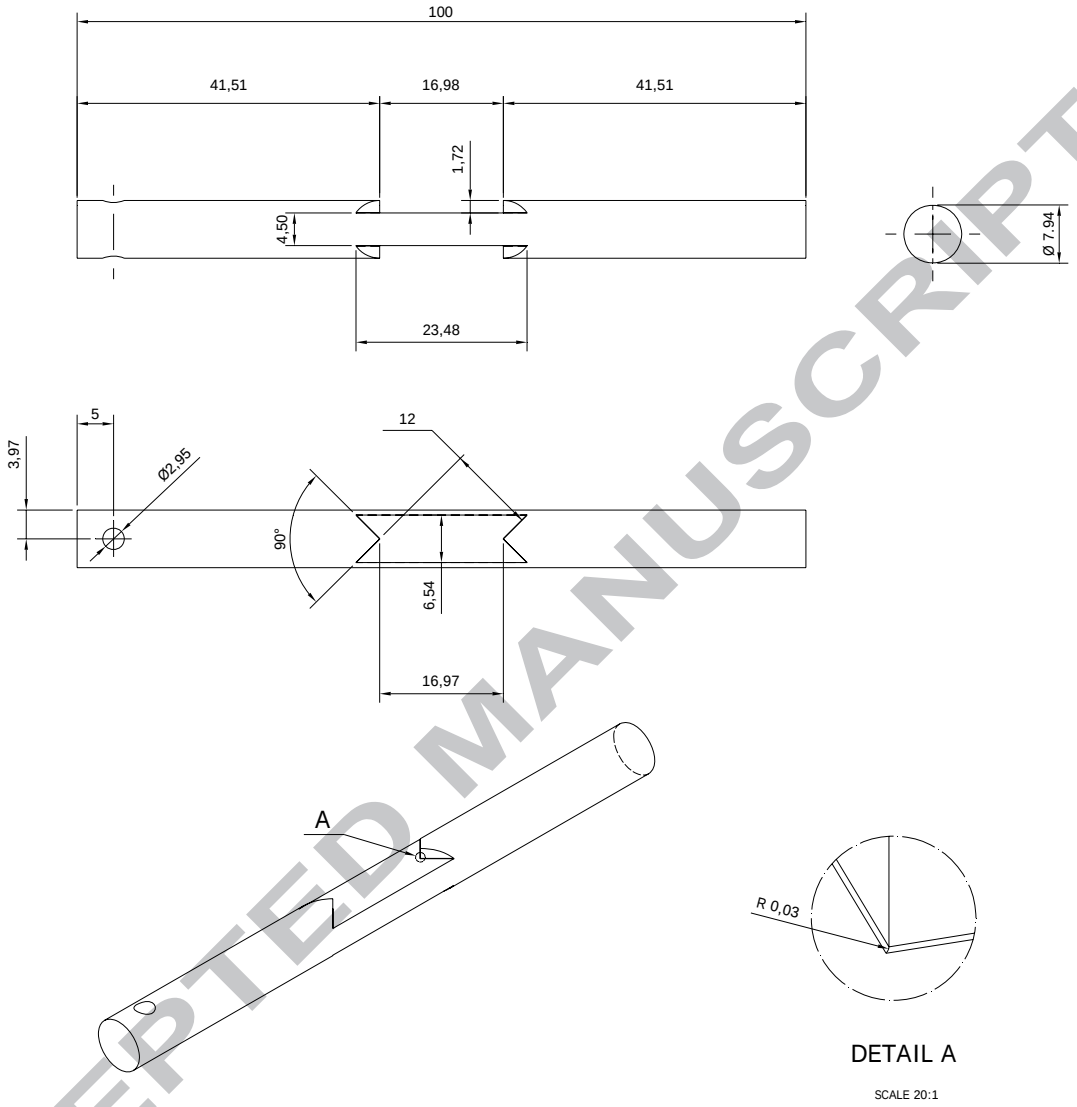

Figure 4. Geometry of the tested specimen.

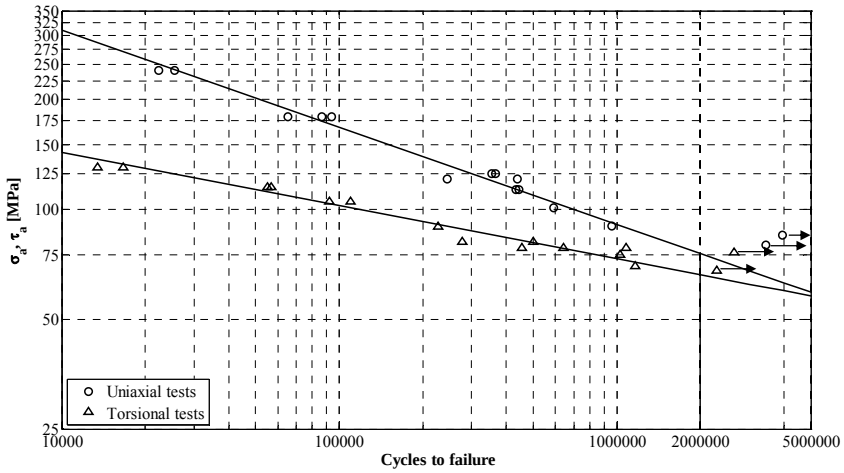

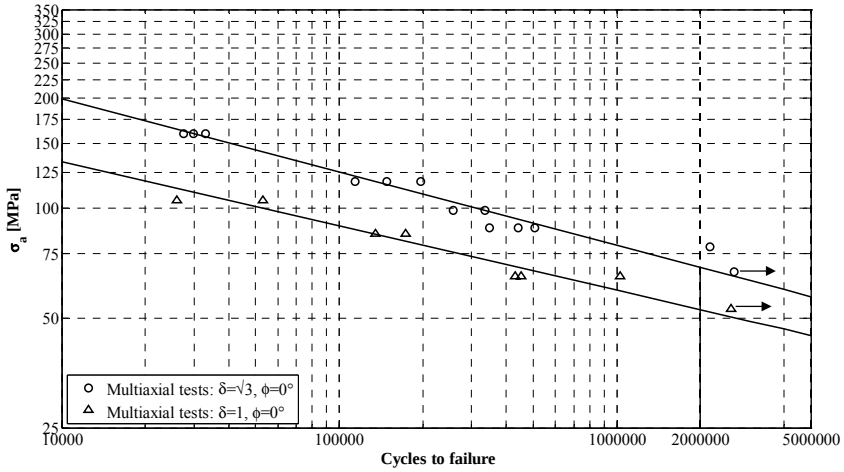

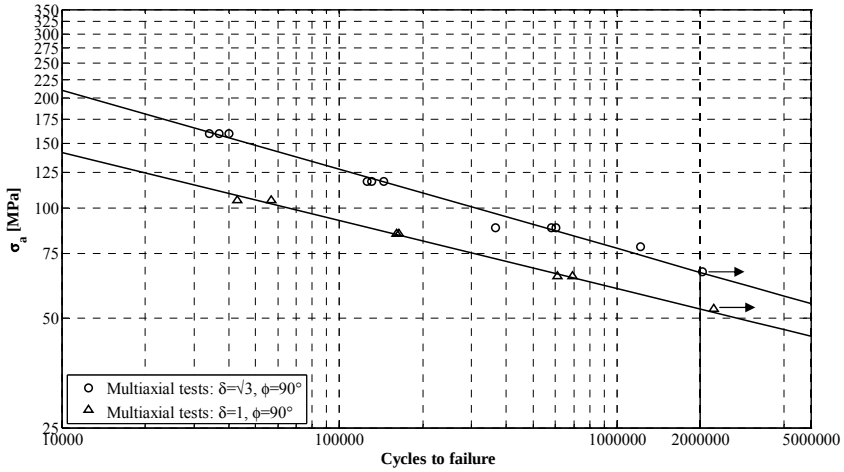

Figure 5. Fatigue date of all series tested.

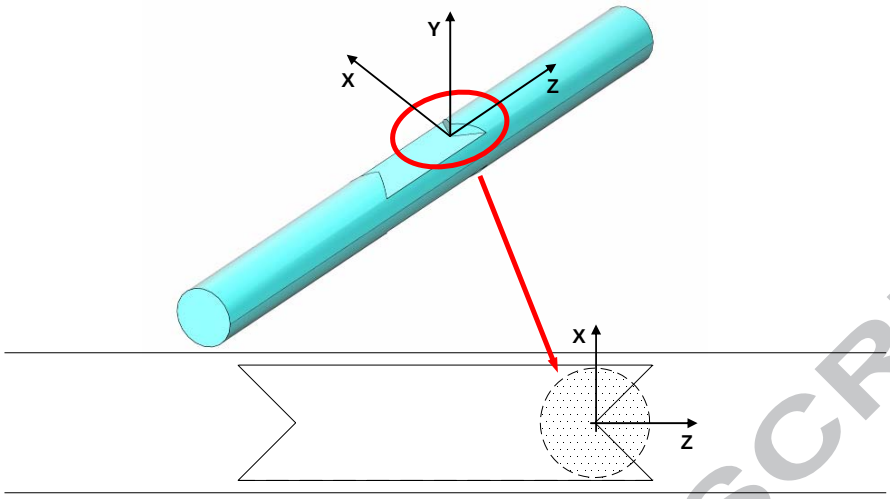

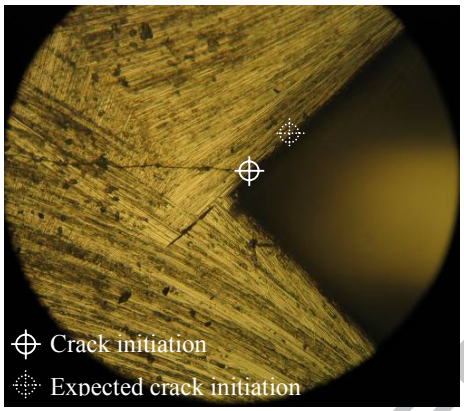

a) Torsional test

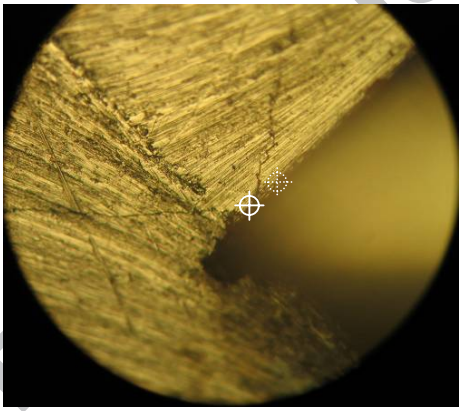

b) Torsional test

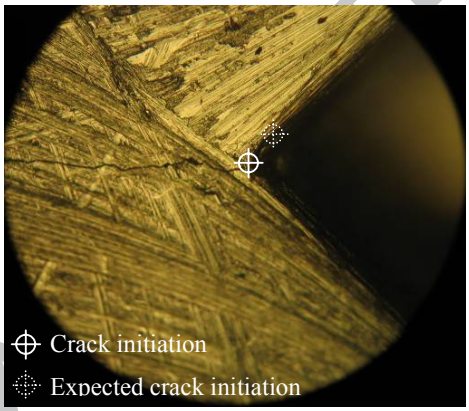

c) Multiaxial test –δ=1, φ=0°

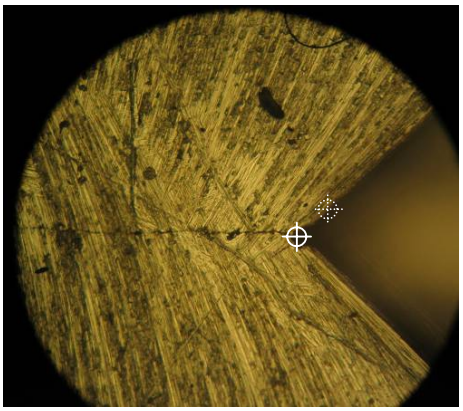

d) Multiaxial test – δ=1, φ=0°

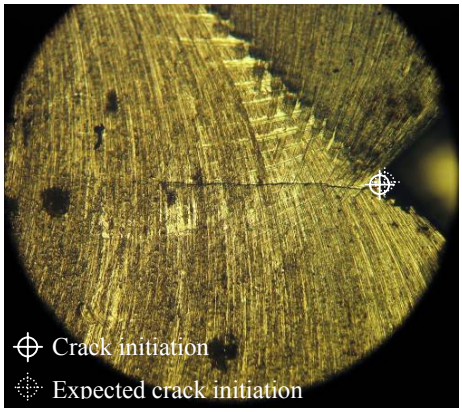

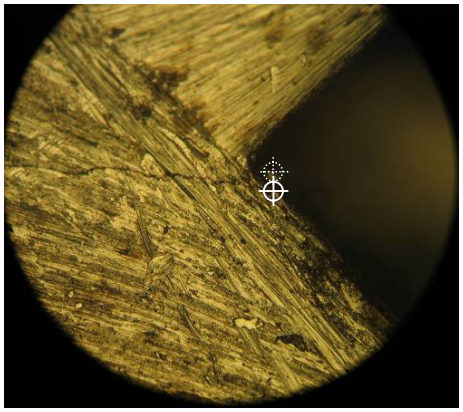

e) Multiaxial test – δ=1, φ=90°

f) Multiaxial test – δ=√3, φ=0°

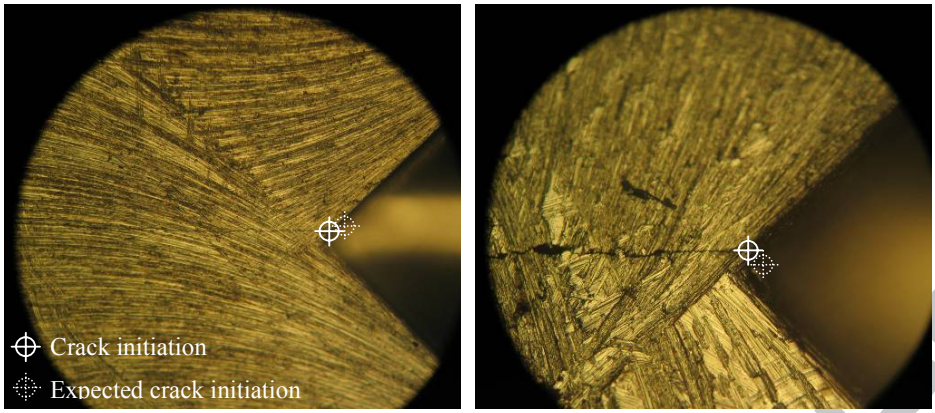

g) Multiaxial test – δ=√3, φ=0°

h) Multiaxial test – δ=√3, φ=90°

Figure 6. Examples of the observed crack path.

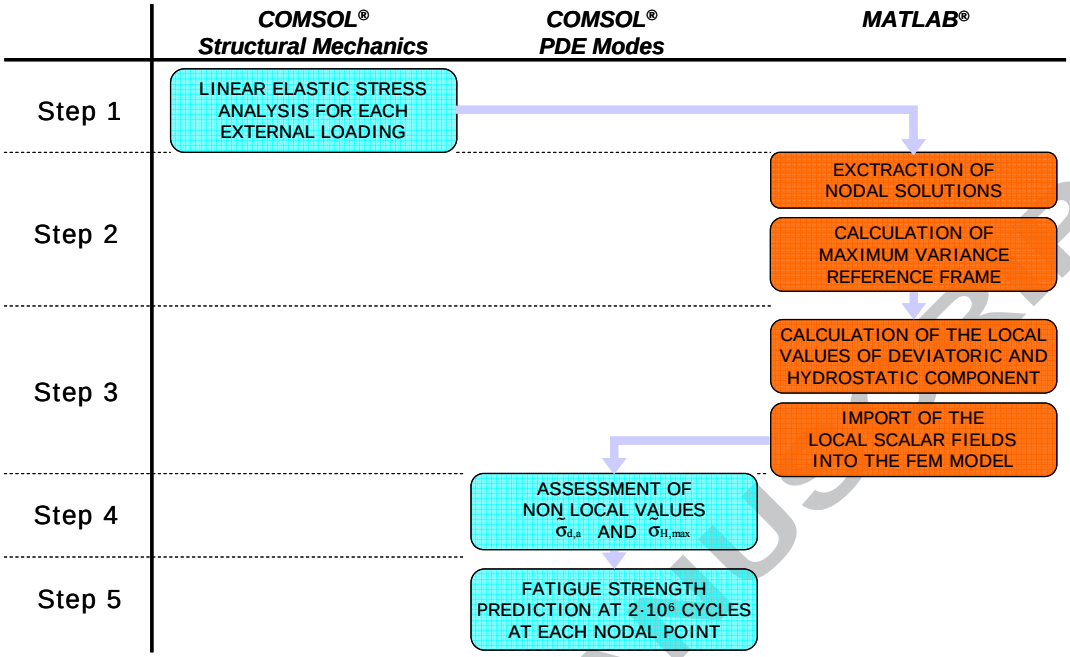

Figure 7. Procedure framework.

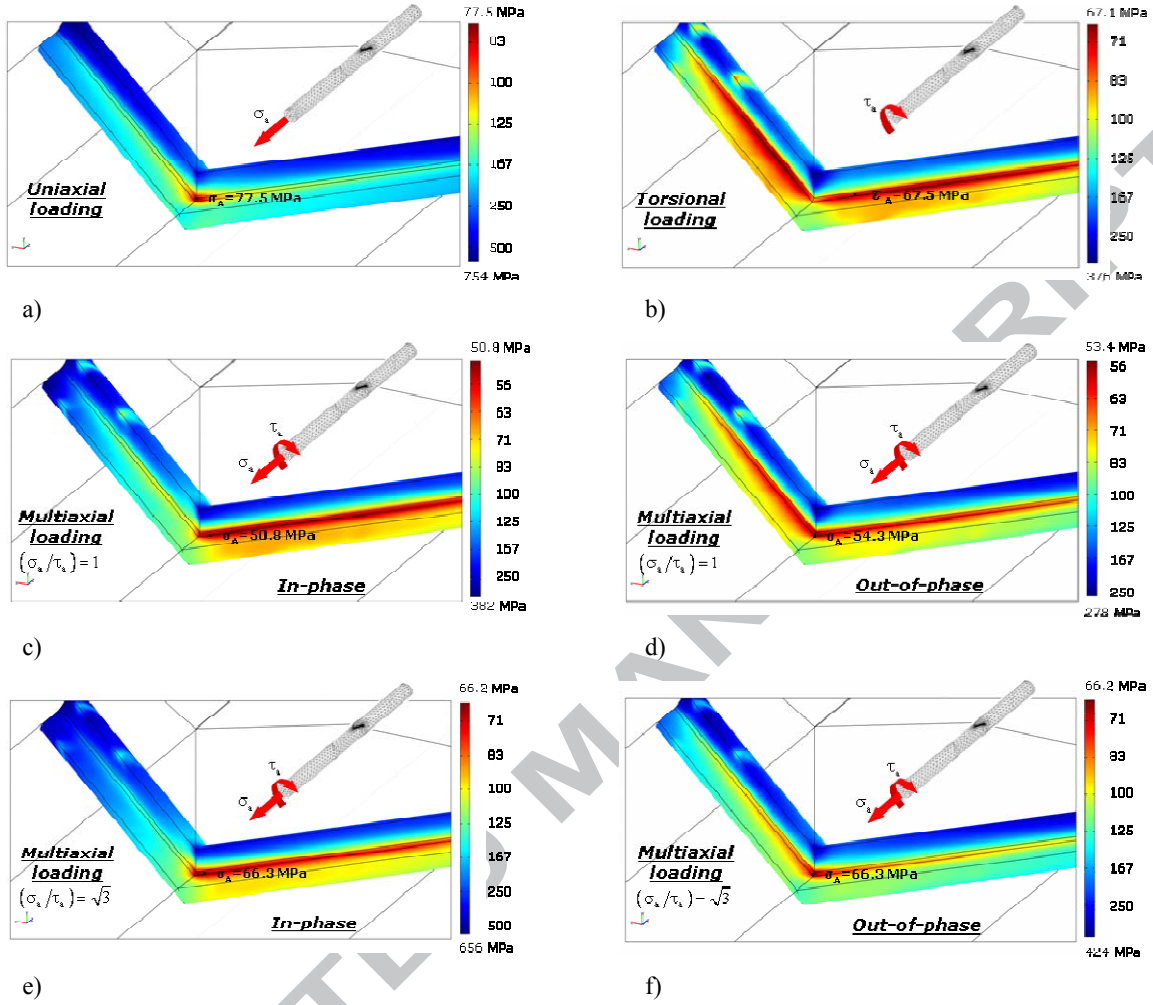

Figure 8. Estimation of nominal stress amplitude to be applied in order to have each nodal point in $2 \cdot 10^6$ cycles strength condition.